



HAL
open science

Revealing the frictional transition in shear thickening suspensions

C Clavaud, A Bérut, B Metzger, Yoel Forterre

► **To cite this version:**

C Clavaud, A Bérut, B Metzger, Yoel Forterre. Revealing the frictional transition in shear thickening suspensions. Proceedings of the National Academy of Sciences of the United States of America, 2017, 114 (20), pp.5147-5152. 10.1073/pnas.1703926114 . hal-01492671

HAL Id: hal-01492671

<https://hal.science/hal-01492671>

Submitted on 20 Mar 2017

HAL is a multi-disciplinary open access archive for the deposit and dissemination of scientific research documents, whether they are published or not. The documents may come from teaching and research institutions in France or abroad, or from public or private research centers.

L'archive ouverte pluridisciplinaire **HAL**, est destinée au dépôt et à la diffusion de documents scientifiques de niveau recherche, publiés ou non, émanant des établissements d'enseignement et de recherche français ou étrangers, des laboratoires publics ou privés.

Revealing the frictional transition in shear thickening suspensions

Cécile Clavaud^{a,1}, Antoine Bérut^a, Bloen Metzger^a, and Yoël Forterre^a

^aAix Marseille Univ, CNRS, IUSTI UMR 7343, 13453 Marseille, France.

This manuscript was compiled on March 8, 2017

Shear thickening in dense particulate suspensions was recently proposed to be driven by the activation of friction above an onset stress arising from short range repulsive forces between particles. Testing this scenario represents a major challenge since classical rheological approaches do not provide access to the frictional properties of suspensions. Here we adopt a new strategy inspired by pressure-imposed configurations in granular flows that specifically gives access to this information. By investigating the quasistatic avalanche angle, compaction, and dilatancy effects in different nonbuoyant suspensions flowing under gravity, we demonstrate that particles in shear-thickening suspensions are frictionless under low confining pressure. Moreover, we show that tuning the range of the repulsive force below the particle roughness suppresses the frictionless state and also the shear-thickening behavior of the suspension. These results, which link microscopic contact physics to the suspension macroscopic rheology, provide direct evidences that the recent frictional transition scenario applies in real suspensions.

| soft matter | shear thickening | dense suspensions | friction |

Discontinuous shear thickening occurs in suspensions whose viscosity dramatically increases, sometimes by several orders of magnitude, when the imposed shear-rate exceeds a critical value [1]. The archetype of such suspensions is cornstarch immersed in water. When sheared vigorously or under impact, these fluids suddenly turn into solids [2]. Such remarkable properties play a key role in the flowing behavior of modern concrete [3] and have motivated applications ranging from soft-body protections to sports equipments [4]. They also offer promising perspectives for the design of smart fluids with tunable rheology [5]. However, the potential realm of development and applications remains largely under-explored due to the lack of understanding of this transition [6].

This situation has moved on very recently owing to new theoretical and numerical works [7, 8]. Since non-Brownian suspensions of hard frictional particles immersed in a viscous fluid are Newtonian, as imposed by dimensional analysis [8–10], the key idea of these studies is to add a short range repulsive force between particles besides hydrodynamics and contact forces. This repulsive force can for instance stem from electrostatic charges or from a specific coating of polymers on the surface of the particle [11]. At small shear rate (or small stress), the repulsive force prevents the grains from touching; the suspension thus flows easily as if particles were frictionless. The viscosity of such a frictionless suspension would diverge at random close packing, whose volume fraction is $\phi_{\text{rcp}} = 0.64$ for monodisperse spheres. Conversely, at large shear rate (or large stress), the repulsive force is overcome by the hydrodynamic forces and particles are therefore pressed into frictional contacts. The viscosity of such a suspension of frictional particles instead diverges at a lower critical volume fraction $\phi_c < \phi_{\text{rcp}}$, with typically $\phi_c \simeq 0.58$ for monodisperse

frictional spheres [9, 10, 12]. In essence, the frictional transition described above brings the suspension closer to its jamming point: this critical volume fraction shift suddenly increases its apparent viscosity.

This scenario has been successfully tested and analyzed in discrete numerical simulations performed for non-Brownian [7, 10] and Brownian [13] suspensions. Supporting results are also provided by recent experimental investigations. For instance, standard rheological measurements were performed on suspensions of small PMMA particles sterically stabilized by a coating of poly-12-hydroxystearic acid [14]. The suspension was indeed found to follow two separate viscosity curves with distinct critical volume fractions, depending on what shear rate was applied. A similar suspension was investigated under shear reversal [15], during which the viscosity first drops to a low value set by hydrodynamics interactions before increasing to a plateau dominated by contact interactions [16]. As expected in such framework, only the contact contribution to the viscosity increases with increasing shear-rate, confirming the key role of contacts in shear thickening suspensions. Another study reported that in shear thickening suspensions, the first normal stress difference changes sign at the transition [17]. This behavior was interpreted as indicating the formation of frictional contacts between particles, although this point is still a matter of debate [10, 18].

These experimental findings are encouraging, however they also reflect a major difficulty in testing the frictional transition put forward in the recent theoretical scenario. The standard rheological techniques used, performed under fixed volume fraction, provide information about the suspension shear rate, shear stress and viscosity. However they do not give access to the suspension friction coefficient, which is here the key quantity one needs to access. In this article, we propose a

Significance Statement

The sudden and severe increase in the viscosity of certain suspensions above an onset stress is one of the most spectacular phenomena observed in complex fluids. This shear thickening, which has major implications for industry, is a long-standing puzzle in soft-matter physics. Recently, a frictional transition was conjectured to cause this phenomenon. Using experimental concepts from granular physics, we provide direct evidences that such suspensions are frictionless under low confining pressure, which is key to understanding their shear thickening behavior.

C.C., A.B., B.M. and Y.F. designed the research, performed the research, analyzed data and wrote the paper.

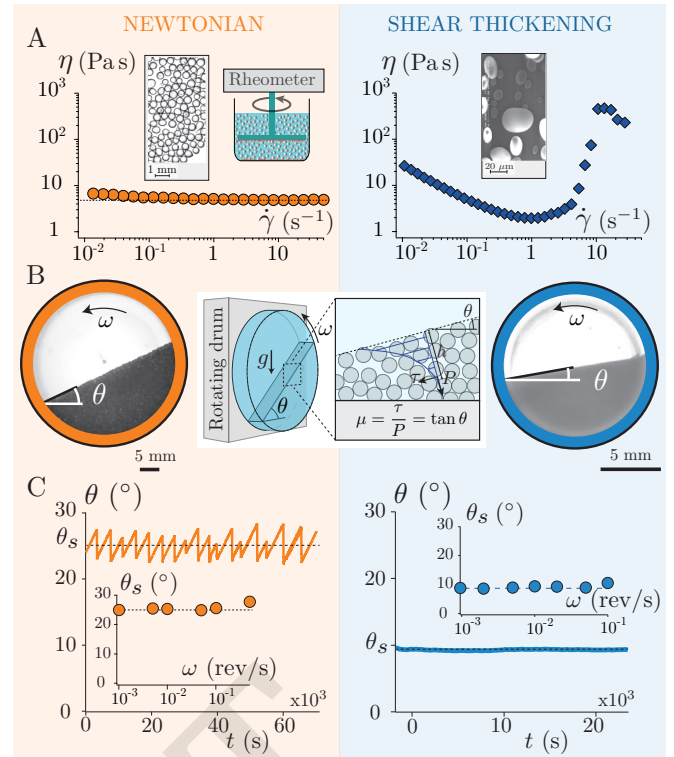
The authors declare no conflict of interest.

¹To whom correspondence should be addressed. E-mail: cecile.clavaud@univ-amu.fr

125 different approach inspired by pressure-imposed experiments
 126 in granular flows [19], which specifically provides access to
 127 the friction coefficient of the suspension. By investigating the
 128 quasistatic avalanche angle, compaction, and dilatancy effects,
 129 in different nonbuoyant suspensions flowing under gravity,
 130 we provide the first direct proof that particles in shear thickening
 131 suspensions are frictionless under low confining pressure. We
 132 then bridge microscopic contact physics to the macroscopic
 133 rheology by tuning the short-range repulsive force in a model
 134 suspension of silica beads. We find that this shear thickening
 135 suspension, which has a frictionless state under low stress, no
 136 longer shear thickens when this frictionless state is suppressed.

137 Results

138 **Steady avalanches.** A simple way to probe the frictional behavior
 139 of a suspension is to measure its quasistatic avalanche angle
 140 in a rotating drum using non-buoyant particles [20, 21].
 141 For sake of clarity, we compared the avalanche angle of a
 142 standard Newtonian suspension made of large frictional glass
 143 beads of diameter $d = 500 \mu\text{m}$ (Fig. 1A left), to that of
 144 a typical shear-thickening suspension made of potato starch
 145 particles ($d = 25 \mu\text{m}$) immersed in water (Fig. 1A right). In
 146 both cases, the particle density ρ_p is larger than that of the
 147 suspending fluid ρ_f and the fluid viscosity η_f is chosen so
 148 that the Stokes number St is low and inertial effects can be
 149 neglected ($St = \sqrt{\rho_p \Delta \rho g d^3} / 18 \eta_f \sim 10^{-2}$ where $\Delta \rho = \rho_p - \rho_f$
 150 and g stands for gravity) [21]. Both suspensions are placed
 151 within a rotating drum as shown on the experimental set-up
 152 illustrated on figure 1B (center). By imposing a slow and
 153 constant rotation speed ω , the non-buoyant grains at the
 154 surface of the pile flow under their own weight forming a
 155 steady avalanche of angle θ on top of a region experiencing
 156 a rigid rotation with the drum [20]. In such a configuration,
 157 the confining pressure acting on the flowing layer of grains is
 158 $P = \phi \Delta \rho g h \cos \theta$ where h is the height of the flowing layer
 159 and ϕ its volume fraction; the corresponding tangential stress is
 160 $\tau = \phi \Delta \rho g h \sin \theta$. In the steady state, the macroscopic
 161 friction coefficient of the suspension μ is directly given by the
 162 avalanche angle since by definition $\mu = \tau / P = \tan \theta$. The
 163 avalanche angle θ thus provides access to the macroscopic
 164 friction coefficient of the suspension μ , which itself depends
 165 monotonically on the particle friction coefficient μ_p [22].
 166 For frictional grains, the macroscopic friction coefficient $\mu \simeq 0.4$
 167 has only a weak dependence on μ_p and yields a typical
 168 avalanche angle $\theta \simeq 25^\circ$ [21]. However, when the interparticle
 169 friction μ_p becomes very small (below 0.1), the macroscopic
 170 friction μ sharply drops. Yet, because of steric constraints,
 171 μ remains finite as $\mu_p \rightarrow 0$. For frictionless spherical
 172 particles ($\mu_p = 0$), discrete simulations predict a
 173 quasistatic macroscopic friction $\mu = 0.105$, corresponding
 174 to a non-zero avalanche angle $\theta = 5.76^\circ$ [23]. Therefore,
 175 measuring the pile angle of steady avalanches constitutes a
 176 simple, yet decisive way to probe the interparticle friction
 177 coefficient in suspensions. Moreover, in this rotating drum
 178 configuration, the slope of the avalanche is set by the
 179 flowing layer of grains which is located near the free surface
 180 of the pile. For the low rotation speeds investigated here,
 181 the thickness of the layer h is of the order of a few
 182 particles diameters ($h \sim 10d$) [24]. This means that the
 183 measure of the avalanche angle gives access to the frictional
 184 state of the grains under very low confining pressure. Typically,
 185 for the potato starch particles, the confining pressure within
 186 the flowing layer



187 **Fig. 1.** Steady avalanches in (left) Newtonian and (right) shear thickening suspensions.
 188 (A) Picture and rheograms (viscosity η versus shear-rate $\dot{\gamma}$) of (left) a Newtonian
 189 suspension of large glass beads and (right) a shear thickening suspension of potato
 190 starch particles. Rheograms were obtained in the configuration sketched on the figure
 191 using density matched suspensions. (B) (center) sketch of the rotating drum. Pictures
 192 of a typical steady avalanche for (left) the glass beads immersed in a mixture of Ucon
 193 oil and water and (right) the potato starch immersed in water. (C) Angle of avalanche
 194 θ versus time for (left) the glass beads (right) the potato starch. Insets: steady state
 195 avalanche angle θ_s versus drum rotation speed ω (see Materials and Methods for
 196 the detailed description of particles, fluids and experimental protocol).

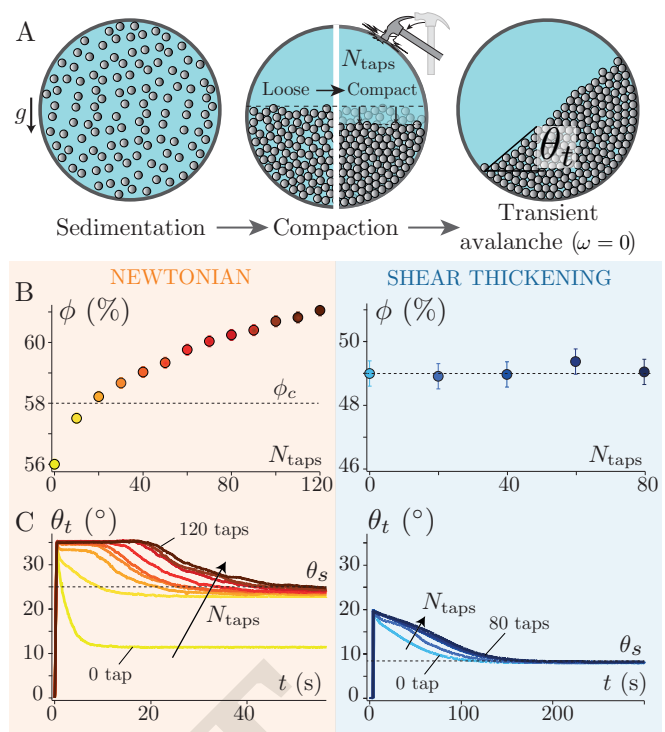
197 is $P \sim 10\phi\Delta\rho g d \simeq 1 \text{ Pa}$.

198 For the Newtonian suspension of large glass beads, the
 199 avalanche angle θ shows classical hysteretic fluctuations [20]
 200 around a time averaged angle $\theta_s \simeq 25^\circ$, see picture on figure
 201 1B (left) and data on figure 1C (left). This angle corresponds
 202 to a suspension friction coefficient $\mu \simeq 0.47$ which is a usual
 203 value for frictional particles. The striking result is that, under
 204 the same flowing conditions, the shear thickening suspension
 205 of potato starch particles yields a much lower avalanche angle,
 206 see picture on figure 1B (right) and data on figure 1C (right).
 207 The suspension can flow steadily with an angle of avalanche as
 208 small as $\theta_s \simeq 8.5^\circ$. This angle corresponds to a suspension
 209 friction coefficient $\mu \simeq 0.15$, showing that the friction coefficient
 210 between particles is nearly vanishing. The suspension friction
 211 coefficient ($\mu \simeq 0.15$) here is slightly larger than the expected
 212 value for frictionless spheres ($\mu = 0.105$) because potato starch
 213 particles are prolate, which geometrically increases the macro-
 214 scopic friction coefficient [25, 26]. Importantly, in the range
 215 of drum rotation speeds ω investigated, the avalanche angles
 216 reported here do not depend on ω (Fig. 1C left and right
 217 insets). They thus characterize the frictional properties of the
 218 suspension in its quasistatic regime, i.e. when the suspension
 219 reaches its critical jamming state [9].

249 **Compaction and dilatancy.** Another robust way to probe the
 250 frictional behavior of a suspension is to investigate compaction
 251 and dilatancy effects [21]. The protocol is the following: parti-
 252 cles are first suspended entirely within the drum before letting
 253 them sediment (Fig. 2A). The sediment is then compacted
 254 by gently hitting the drum with a rubber head hammer N_{taps}
 255 times. The volume fraction ϕ of the sediment (the ratio of
 256 the particles volume to the total volume of the sediment) is
 257 measured throughout this compaction process. Finally, the
 258 drum is quickly rotated by a fixed angle $\theta_s + 10^\circ$ above the
 259 steady state avalanche angle, to generate a transient avalanche
 260 whose angle θ_t is measured versus time.

261
 262 A conspicuous feature of frictional systems, such as a pile
 263 of large glass beads, is that it compacts under vibrations.
 264 As shown on figure 2B (left), the packing fraction of the
 265 glass beads sediment, which right after sedimentation starts
 266 from a loose state ($\phi = 0.56 < \phi_c$), progressively increases
 267 with the number of taps to eventually reach a dense state
 268 ($\phi = 0.61 > \phi_c$). Remarkably, within this frictional system,
 269 very different transient avalanches are observed depending on
 270 the initial preparation of the sediment (Fig. 2C left). For an
 271 initial loose packing (0 tap), the avalanche rapidly flows until
 272 its angle relaxes to an angle much lower than θ_s (the steady
 273 state avalanche angle measured earlier). Conversely, for an
 274 initially compact sediment (120 taps), one observes a long
 275 delay during which the avalanche stays still. It then slowly
 276 flows, relaxing to θ_s . Such a drastic change in the avalanche
 277 dynamics with the packing of the initial sediment relies on a
 278 well known pore pressure feedback mechanism [27–29], which
 279 only applies for dilatant (i.e. frictional) systems [23]. As first
 280 described by Reynolds [30], deformation of a dense granular
 281 packing of frictional grains requires its dilation. Thus, as the
 282 drum is tilted for the avalanche to flow, the initially compact
 283 sediment must dilate. However, dilation in the presence of an
 284 incompressible interstitial fluid induces a fluid flow: some fluid
 285 is sucked within the granular network. This fluid flow presses
 286 the grains against each other, thereby enhancing friction. As a
 287 result, for a compact pile of frictional grains, the avalanche is
 288 strongly delayed and then flows slowly relaxing to θ_s [28, 31].
 289 Conversely, a loosely packed granular bed tends to compact
 290 when it deforms. This time, the interstitial fluid is expelled
 291 from the granular packing, thereby resulting in a fluidization
 292 of the grains: the avalanche flows rapidly and relaxes to an
 293 angle smaller than θ_s .

294
 295 The compaction and dilatancy effects observed for the large
 296 glass beads are the phenomenological signature of frictional
 297 grains. For frictionless particles, the situation is markedly
 298 different since there is only one possible state of compaction
 299 ($\phi_c = \phi_{rcp}$) and no dilatancy effects are thus expected under
 300 shear [23]. This is precisely what we observe with the shear-
 301 thickening suspension of potato starch particles: tapping the
 302 settled bed of potato starch particles does not modify its pack-
 303 ing fraction (Fig. 2B right) and hardly changes the dynamic of
 304 the transient avalanches which all relax to θ_s (Fig. 2C right).
 305 These experiments again show that, under low confining pres-
 306 sure, potato starch particles behave as if they were frictionless.
 307 Note that the maximum packing fraction of the potato starch
 308 particles, $\phi = 49\%$, may seem small. However this low value
 309 can be explained by the anisotropic shape of the particles and
 310 also their tendency to swell when immersed in water [32].



311
 312
 313
 314
 315
 316
 317
 318
 319
 320
 321
 322
 323
 324
 325
 326
 327
 328
 329
 330
 331
 332
 333
 334
 335
 336
 337
 338
 339
 340
 341
 342
 343
 344
 345
 346
 347
 348
 349
 350
 351
 352
 353
 354
 355
 356
 357
 358
 359
 360
 361
 362
 363
 364
 365
 366
 367
 368
 369
 370
 371
 372

Fig. 2. Compaction and transient avalanches in (left) Newtonian and (right) shear thickening suspensions. (A) Sketch of the experimental protocol to study compaction and dilatancy effects. (B) Volume fraction of the sediment ϕ versus number of taps N_{taps} (left) for the large glass beads and (right) for the potato starch particles. (C) Angle of the transient avalanche θ_t versus time obtained for different initial compactions of the sediment (left) for the large glass beads and (right) for the potato starch particles.

Tuning microscopic friction using a model suspension. We have shown that potato starch particles immersed in water produce a shear thickening rheology and are frictionless under low confining pressure. These results are consistent with the frictional transition scenario for shear thickening presented in the introduction [7, 8]. They suggest the existence of a short range repulsion force or a microscopic pressure-dependent friction between the starch particles. However, the origin of this force and more generally the surface physico-chemistry of starch remain unclear [6, 33, 34]. To vary the interaction force between particles and investigate the frictional transition within a well-controlled system, we turn to a model suspension composed of silica beads immersed in water (Fig. 3A top). We use non-Brownian silica particles of diameter $d = 24 \mu\text{m}$ comparable in size to the starch particles. When immersed in water, such silica particles spontaneously develop negative surface charges, which generates an electrostatic repulsive force between the grains [35–37]. Moreover, this surface charge can easily be screened by dissolving electrolytes (salt) within the solvent. Increasing the salt concentration decreases the range of the repulsive force, i.e. the Debye length λ_D (Fig. 3A bottom). This model system is thus particularly appealing to test the recent frictional transition scenario and clarify the link between microscopic interactions between particles, friction, and the suspension macroscopic rheology.

We first use the rotating drum to systematically investigate steady avalanches, compaction and dilatancy effects on two suspensions of silica beads: one with silica beads immersed

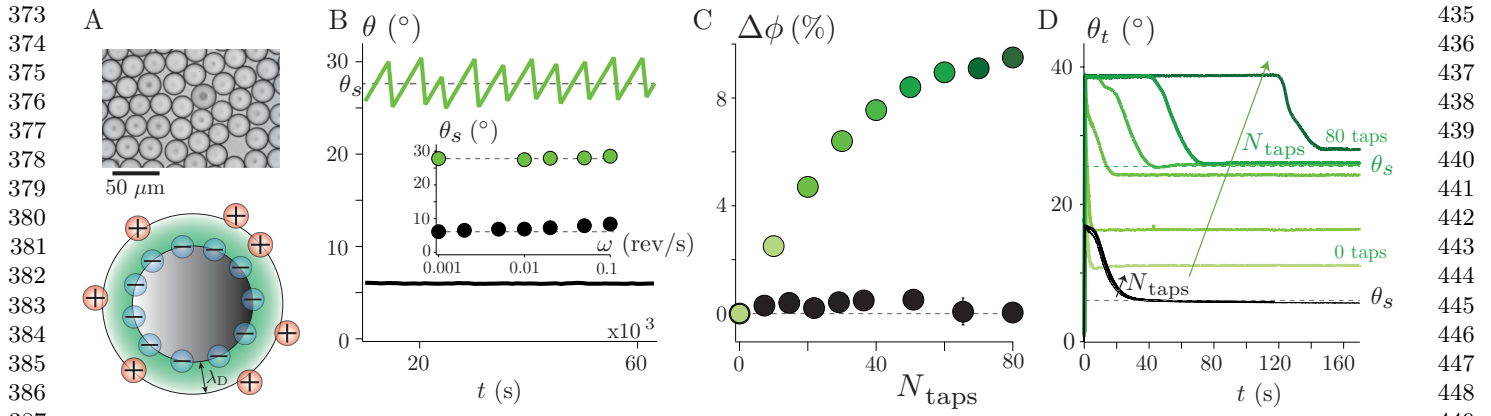


Fig. 3. Steady avalanches, compaction and dilatancy effects in suspensions of silica beads in pure water (black) or ionic solution (green). (A) Picture of the silica particles and sketch of a silica bead immersed in an ionic solution. Silica particles spontaneously carry negative charges on their surface when immersed in water. The range of the resulting repulsive force, i.e. the Debye length λ_D , can be tuned by changing the ionic concentration of the solvent. (B) Pile slope avalanche angle θ versus time, (C) relative packing fraction of the sediment $\Delta\phi = \phi(N_{\text{taps}}) - \phi(N_{\text{taps}} = 0)$ versus number of taps and (D) transient avalanche angle θ_t versus time for the silica beads in (green) a sodium chloride solution with $[\text{NaCl}] = 0.1 \text{ mol L}^{-1}$ and (black) in pure water.

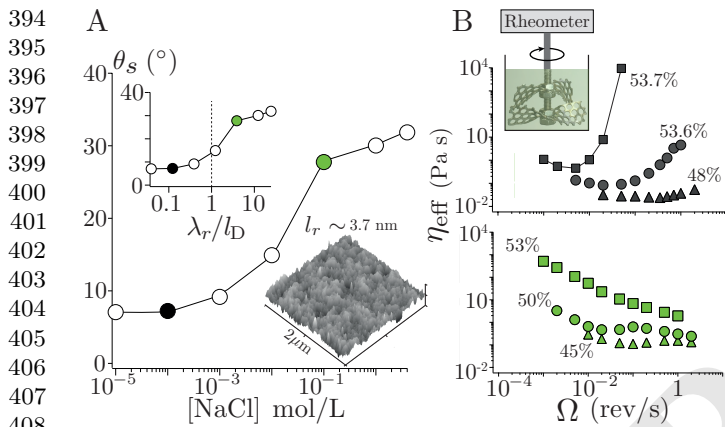


Fig. 4. Frictional transition in silica suspensions when varying the range of the repulsive force and link with macroscopic rheology. (A) Steady avalanche angle θ_s versus salt concentration $[\text{NaCl}]$. Top inset: steady avalanche angle θ_s versus particle roughness normalized by the Debye Length l_r/λ_D . Bottom inset: AFM scan of a silica particle surface. The peak roughness is $l_r = 3.73 \pm 0.80 \text{ nm}$. (B) Rheograms of silica beads suspensions obtained for different volume fractions in solutions of water and NaCl with salt concentration (top) $[\text{NaCl}] = 10^{-4} \text{ mol L}^{-1}$ and (bottom) $[\text{NaCl}] = 0.1 \text{ mol L}^{-1}$. The effective viscosity is $\eta_{\text{eff}} = \alpha\Gamma/(2\pi\Omega L^3)$, where Γ is the torque, Ω the revolution speed and $\alpha \simeq 2.07$ is a calibration constant. Inset: sketch of the experimental configuration used to obtain the rheograms.

in pure water, and the second with the beads immersed in a solution of water and NaCl with a large concentration of salt ($[\text{NaCl}] = 0.1 \text{ mol L}^{-1}$) to fully screen the Debye layer. Here again inertia is negligible ($St \sim 5 \cdot 10^{-3}$) and the flowing regime is quasistatic ($\omega \rightarrow 0$). As illustrated on figure 3B,C and D (green data), in the presence of a large concentration of salt which screens the repulsive force, the suspension behaves as frictional. The steady state avalanche angle is large: $\theta_s \simeq 27.5^\circ$, the packing fraction of the sediment evolves from a loose packing right after sedimentation to a dense packing*

*The absolute volume fraction is not reported in Fig. 3 since here it depends on the system size. This size effect can be explained by the large value of the Debye length in pure water ($\lambda_D \simeq 1 \mu\text{m}$), which is not negligible relative to the silica particle diameter [38]. Here, particles may be thought of as a hard core of diameter d surrounded by a soft crust of thickness equal to the Debye length. The maximum packing of such system, when the confining pressure $P \rightarrow 0$, is $\phi_{\text{max}} \simeq \phi_{\text{rcp}}(1 - 3\lambda_D/d) \simeq 0.48$. However, due to the hydrostatic pressure within the

after 80 taps, and the dynamics of the transient avalanche strongly depends on the initial packing, showing features related to the dilatancy effects discussed earlier. Conversely, the silica beads in pure water behave as frictionless particles (Fig. 3B,C and D, black data). The steady state avalanche angle is $\theta_s \simeq 6^\circ$. This value is remarkably close to the quasistatic macroscopic friction angle obtained numerically for ideal frictionless spheres $\theta_s = 5.76^\circ \pm 0.22$ [23]. Additionally, no compaction of the granular bed and no discernable effect of the initial packing on the transient avalanches are observed. These results clearly demonstrate that the presence of a short range repulsive force can lead under low stress to a frictionless behavior of the particles.

To further inquire about the microscopic origin of this frictionless behavior under low stress, we measured the steady avalanche angle θ_s as a function of the salt concentration $[\text{NaCl}]$. Figure 4A shows that the suspension transits progressively from frictionless, with $\theta_s \simeq 6^\circ$, in pure water to frictional with $\theta_s \simeq 30^\circ$ when the salt concentration $[\text{NaCl}]$ is increased. Besides this macroscopic measurement, we also characterized the particle roughness with an AFM and found that the peak roughness of the silica particles is $l_r = 3.73 \pm 0.80 \text{ nm}$. Since the Debye length is entirely set by the salt concentration: $\lambda_D = 0.304/\sqrt{[\text{NaCl}]} \text{ nm}$ (at $T = 25^\circ \text{C}$) [36], we can plot the steady avalanche angle θ_s as a function of l_r/λ_D (Fig. 4A top inset). Interestingly, the transition from frictionless to frictional occurs for $l_r/\lambda_D \sim 1$. This result strongly supports the idea that the frictionless state arises from the interparticle repulsive force caused by the electrostatic double layer. When its range is smaller than the particle roughness, this force becomes ineffective to prevent the grains from touching and the system is frictional. According to the scenario described in the introduction [7, 8], the frictional transition should occur when the confining pressure P exerted by the weight of the granular layer equals the critical pressure P_c which the short range repulsive forces can sustain. Assuming that the repulsive force follows an exponential decay as $F_{\text{rep}}(z) = F_0 \exp(-z/\lambda_D)$ [36], where z is the distance between

granular bed which depends on the system size, grains deep in the bed must be closer from each other than those at the top. The absolute volume fraction may thus lie anywhere between the latter value and 0.64 (random close packing), depending on the system size.

497 the particles surfaces, the critical pressure at contact $z = 2l_r$
498 writes $P_c \sim F_{\text{rep}}(2l_r)/(\pi d^2/4) \sim (4F_0/\pi d^2) \exp(-2l_r/\lambda_D)$.
499 Matching it to the confining pressure $P \sim 10\phi\Delta\rho gd$ predicts
500 a transition when $l_r/\lambda_D \sim -(1/2) \log(10\phi\Delta\rho gd^3/4F_0)$. Us-
501 ing $F_0/d \sim 1$ mN/m as reported for silica surfaces in NaCl
502 electrolytes [35] yields $l_r/\lambda_D \simeq 1.9$, in fair agreement with the
503 transition observed on figure 4A.

504 Finally, we investigate whether for this model suspension,
505 the existence of a frictionless state under low confining pressure
506 leads to a shear thickening rheology and if the elimination of
507 this state (by screening repulsive forces) restores a Newtonian
508 behavior. Rheograms of the silica suspensions were obtained
509 using the configuration sketched on the inset of figure 4B. Since
510 silica particles are denser than the aqueous suspending fluid,
511 we used a double-helix with tilted blades shearing the entire
512 sample to avoid sedimentation and maintain the homogeneity
513 of the suspension during the measurement. We then define
514 an effective viscosity $\eta_{\text{eff}} = \alpha\Gamma/(2\pi\Omega L^3)$ given by the ratio
515 of the effective stress Γ/L^3 , where Γ is the torque and L the
516 helix diameter, to the effective shear rate $2\pi\Omega$ given by the
517 revolution speed Ω of the helix. The constant $\alpha \simeq 2.07$ is
518 set to ensure that the effective viscosity matches the actual
519 viscosity for a newtonian fluid. We performed rheological
520 measurements on two suspensions of silica particles immersed
521 in water with a salt concentration $[\text{NaCl}] = 10^{-4} \text{ mol L}^{-1}$ and
522 $[\text{NaCl}] = 10^{-1} \text{ mol L}^{-1}$ respectively, i. e. just before and after
523 the frictional transition observed on figure 4A. First, we find
524 that the suspension which has a frictionless state under low con-
525 fining pressure displays all the features of a shear-thickening
526 suspension (Fig. 4B top): continuous shear thickening is
527 observed at moderate volume fractions, while larger volume
528 fractions lead to a dramatic increase of its effective viscosity
529 (by about 4 orders of magnitude). Second, the striking result is
530 that when the repulsive force is screened, so that no frictionless
531 state exists under low confining pressure, the same suspension
532 no longer shear-thickens (Fig. 4B bottom). These measure-
533 ments corroborate previous rheological characterizations using
534 Brownian silica microspheres [17, 39, 40] and confirm the link
535 between the existence of a repulsive force, friction and shear
536 thickening rheology.

537 Discussion

538 In this article we propose a pressure-imposed approach, in-
539 spired from experiments in granular flows, to directly probe
540 the microscopic frictional properties of non-Brownian shear
541 thickening suspensions. By systematically investigating steady
542 avalanches, compaction, and dilatancy effects, in rotating
543 drums experiments, we provide the first direct proof that
544 shear thickening suspensions have a frictionless state under
545 low confining pressure. Unlike Newtonian suspensions of fric-
546 tional particles [9, 20, 28, 29], shear thickening suspensions
547 under low stress flow with a very small avalanche angle, do not
548 compact and show no dilatancy effect. This phenomenology
549 clearly indicates the absence of friction between particles [23].
550 Moreover, by using a model suspension of negatively charged
551 silica beads, we find that lowering the range of the repulsive
552 force below the particle roughness makes the suspension tran-
553 sit from a frictionless to frictional state. The elimination of
554 this frictionless state under low confining pressure also sup-
555 presses the shear thickening behavior of the suspension. These
556 experimental results, by linking microscopic contact physics to

557 the suspension macroscopic rheology, provide strong evidences
558 that the frictional transition scenario [7, 8] recently proposed
559 to explain shear thickening, applies in real suspensions. For
560 discontinuous shear thickening to occur, the presence of short
561 range repulsive forces able to prevent inter-particle friction at
562 low stress thus seems essential. This picture contrasts with
563 other models of shear thickening in which idealized lubrica-
564 tion hydrodynamics [41], confinement effects [42], particule
565 migration phenomena [43] or inertia [44, 45] were put forward.

566 The rotating drum configuration used in our study pro-
567 vides a simple, yet robust way to characterize inter-particle
568 friction of dense non-buoyant suspensions. Nevertheless, this
569 configuration also has some limitations. When slowly rotat-
570 ing the drum filled with a non-buoyant suspension, the thin
571 flowing layer is on top of a pile experiencing solid rotation.
572 Particles thus remain in static contact during long times. For
573 microparticles coated with polymers, which are often involved
574 in shear thickening, these enduring contacts may age and lead
575 to cohesion between grains. In this case, the avalanche angle
576 is no longer constant [46, 47]. In our experiments performed
577 with silica particles, small adhesive forces may have affected
578 our results as they could for instance explain the slightly large
579 avalanche angles measured at high salt concentrations (Fig. 3
580 and 4). However, the transition from low to high avalanche
581 angles must be dominated by frictional effects as (i) the steady
582 avalanche angle saturates as the salt concentration is increased,
583 (ii) the avalanches have a constant slope from the top to the
584 bottom of the avalanche unlike adhesive powders, (iii) adhe-
585 sion alone without friction would not lead to the dilatancy
586 effects observed on figure 3D.

587 Finally, we emphasize that the rotating drum configuration
588 gives access to the grains frictional properties in the limit of
589 low confining pressure ($P \rightarrow 0$) and in the quasistatic regime, i.
590 e. when the viscous number of the suspension $\mathcal{J} = \eta_f \dot{\gamma}/P \rightarrow 0$.
591 Interestingly, we were still able to evidence the frictional tran-
592 sition predicted in the recent model by lowering the critical
593 pressure P_c while the confining pressure P remained fixed (see
594 Fig. 4A). To fully explore the recent models, this transition
595 should also be addressed by varying P while keeping P_c con-
596 stant, and also by varying the viscous number \mathcal{J} . Recently,
597 promising devices have been developed opening the route to
598 pressure-imposed rheometry of dense suspensions, but they are
599 so far limited to the study of macroscopic particles [9]. Extend-
600 ing such pressure-imposed approaches to suspensions of shear
601 thickening and colloidal particles represents a challenging, yet
602 very exciting issue for future studies.

603 Materials and Methods

604 **Particles.** The grains used in figure 1 and 2 (left) for the Newtonian
605 suspension are large glass beads of diameter $d = 487 \pm 72 \mu\text{m}$ and
606 density $\rho_p = 2500 \text{ kg m}^{-3}$. The grains used in figure 1 and 2 (right)
607 for the shear thickening suspension are potato starch particles of
608 major axis $d = 25 \pm 15 \mu\text{m}$ and (dry) density $\rho_p = 1500 \text{ kg m}^{-3}$. The
609 silica beads used in figure 3 and figure 4 are commercial particles
610 from Microparticles GmbH with diameter $23.46 \pm 1.06 \mu\text{m}$ and
611 density $\rho_p = 1850 \text{ kg m}^{-3}$.

612 **Rotating drums experiments.** The drum used for the large glass
613 beads (Fig. 1B left) has a diameter of 52mm and a depth of
614 10mm with a coarsened side wall. It is filled with a mixture of
615 Ucon oil and pure (micro-filtered) water of viscosity $\eta_f = 57 \text{ mPas}$
616 and density $\rho_f = 1005 \text{ kg m}^{-3}$. The drum used for potato starch
617

(Fig. 1B right) and silica particles (Fig. 3 and 4) has a diameter of 12 mm and a depth of 3 mm with a coarsened side wall. It is filled with pure water or sodium chloride solutions. Note that to avoid aging of the potato starch, the small drum was surrounded by a thermal bath maintaining its temperature at 7°C. The drums were mounted on a precision rotating stage (M-061PD from PI piezo-nano positioning). To perform the experiment, the grains were first suspended by rotating the drum at 90°s^{-1} . Then, the rotating speed ω was set to the desired value and pictures were taken using a Nikon D300S camera. Compaction experiments, in figures 2 and 3, consisted in dropping a rubber head hammer on the drum always from the same height in sequences of 10 taps. Between each sequence, a waiting time was respected to let the system relax. The relative variation of the packing fraction $\Delta\phi$ was inferred by image analysis from the variation of the area of the granular bed.

Rheological measurements. The rheograms of figure 1 were obtained in the configuration sketched in the inset of that figure. To perform rheological measurements with a large gap (up to 10 mm required for the large glass beads) in a plane-plane geometry, the top plate (diameter 50 mm) is fully immersed in the suspension, which itself is contained in a cylindrical vessel (diameter 60 mm). In both cases, the particles were density matched with the suspending fluid to avoid sedimentation. For the large glass beads, the suspending fluid was a mixture of water (30 % wt), glycerol (13 % wt) and sodium polytungstate (57 % wt). For the potato starch, it was a mixture of water (45 % wt) and cesium chloride (55 % wt). The viscosity is obtained from increasing and decreasing ramps of shear rate after

a pre-shear. No migration effects were noticeable. The rheograms of figure 4B were obtained in a different configuration since the need to control physico-chemistry (salt concentration) does not allow us to match the suspending fluid density. The configuration, sketched in the inset of figure 4B, uses a double-helix with tilted blades shearing the entire sample to maintain the homogeneity of the suspension during the measurement. The suspension volume fraction is controlled by first letting the particles settle down and adjusting the liquid level at the pile interface, which defined the packing fraction in the loose state, then adding a given amount of liquid. For each measurement, the suspension is first thoroughly resuspended at a high rotation rate (1 rev/s) while vibrating the container to prevent shear thickening [5]. The rotation rate is then set to a given value and the constant torque is measured before the effect of sedimentation is observed. In all cases, torques and rotation rates were measured using an Anton-Paar MCR 501 rheometer.

ACKNOWLEDGMENTS. We are thankful to Sarah Hormozy and Pauline Dame for helping us with preliminary experiments, Alain Rangis from CINAM for performing the AFM measurements and our technical staffs at IUSTI for building the experiments. This work was supported by the European Research Council under the European Union Horizon 2020 Research and Innovation programme (ERC grant agreement No. 647384) and by the Labex MEC (ANR-10-LABX-0092) under the A*MIDEX project (ANR-11-IDEX-0001-02) funded by the French government program Investissements d'Avenir.

1. Barnes H (1989) Shear-thickening ("dilatancy") in suspensions of nonaggregating solid particles dispersed in newtonian liquids. *Journal of Rheology* 33(2):329–366.
2. Waitukaitis SR, Jaeger HM (2012) Impact-activated solidification of dense suspensions via dynamic jamming fronts. *Nature* 487(7406):205–209.
3. Fernandez N (2014) *From Tribology to Rheology: Impact of interparticle friction in the shear thickening of non-Brownian suspensions*, PhD dissertation. (ETH–Zürich).
4. Wagner NJ, Brady JF (2009) Shear thickening in colloidal dispersions. *Physics Today* 62(10):27–32.
5. Lin NY, Ness C, Cates ME, Sun J, Cohen I (2016) Tunable shear thickening in suspensions. *Proceedings of the National Academy of Sciences* 113(39):10774–10778.
6. Brown E, Jaeger HM (2014) Shear thickening in concentrated suspensions: phenomenology, mechanisms and relations to jamming. *Reports on Progress in Physics* 77(4):046602.
7. Seto R, Mari R, Morris JF, Denn MM (2013) Discontinuous shear thickening of frictional hard-sphere suspensions. *Phys. Rev. Lett.* 111:218301.
8. Wyart M, Cates ME (2014) Discontinuous shear thickening without inertia in dense non-brownian suspensions. *Phys. Rev. Lett.* 112:098302.
9. Boyer F, Guazzelli É, Pouliquen O (2011) Unifying suspension and granular rheology. *Physical Review Letters* 107(18):188301.
10. Mari R, Seto R, Morris JF, Denn MM (2014) Shear thickening, frictionless and frictional rheologies in non-brownian suspensions. *Journal of Rheology* 58(6):1693–1724.
11. Lee S, Spencer ND (2008) Sweet, hairy, soft, and slippery. *Science (Washington, DC, United States)* 319(5863):575–576.
12. Silbert LE (2010) Jamming of frictional spheres and random loose packing. *Soft Matter* 6(13):2918–2924.
13. Mari R, Seto R, Morris JF, Denn MM (2015) Discontinuous shear thickening in brownian suspensions by dynamic simulation. *Proceedings of the National Academy of Sciences* 112(50):15326–15330.
14. Guy BM, Hermes M, Poon WCK (2015) Towards a unified description of the rheology of hard-particle suspensions. *Phys. Rev. Lett.* 115:088304.
15. Lin NYC et al. (2015) Hydrodynamic and contact contributions to continuous shear thickening in colloidal suspensions. *Phys. Rev. Lett.* 115:228304.
16. Blanc F, Peters F, Lemaire E (2011) Local transient rheological behavior of concentrated suspensions. *Journal of Rheology* 55(4):835–854.
17. Royer JR, Blair DL, Hudson SD (2016) Rheological signature of frictional interactions in shear thickening suspensions. *Phys. Rev. Lett.* 116:188301.
18. Cwalina CD, Wagner NJ (2014) Material properties of the shear-thickened state in concentrated near hard-sphere colloidal dispersions. *Journal of Rheology* 58(4):949–967.
19. Forterre Y, Pouliquen O (2008) Flows of dense granular media. *Annu. Rev. Fluid Mech.* 40:1–24.
20. Courrech du Pont S, Gondret P, Perrin B, Rabaud M (2003) Granular avalanches in fluids. *Physical review letters* 90(4):044301.
21. Andreotti B, Forterre Y, Pouliquen O (2013) *Granular media: between fluid and solid*. (Cambridge University Press).
22. Chialvo S, Sun J, Sundaresan S (2012) Bridging the rheology of granular flows in three regimes. *Phys. Rev. E* 85:021305.
23. Peyneau PE, Roux JN (2008) Frictionless bead packs have macroscopic friction, but no dilatancy. *Phys. Rev. E* 78:011307.
24. GDRMiDi (2004) On dense granular flows. *The European Physical Journal E* 14(4):341–365.
25. Azéma E, Radjai F (2010) Stress-strain behavior and geometrical properties of packings of elongated particles. *Physical Review E* 81(5):051304.
26. Guo Y, Wassgren C, Hancock B, Ketterhagen W, Curtis J (2013) Granular shear flows of flat disks and elongated rods without and with friction. *Physics of Fluids* 25(6):063304.
27. Iverson RM (1997) The physics of debris flows. *Reviews of geophysics* 35(3):245–296.
28. Pailha M, Nicolas M, Pouliquen O (2008) Initiation of underwater granular avalanches: Influence of the initial volume fraction. *Physics of Fluids* 20(11):111701.
29. Jerome JJS, Vandenbergh N, Forterre Y (2016) Unifying impacts in granular matter from quicksand to cornstarch. *Physical Review Letters* 117(9):098003.
30. Reynolds O (1885) LVII. On the dilatancy of media composed of rigid particles in contact. With experimental illustrations. *The London, Edinburgh, and Dublin Philosophical Magazine and Journal of Science* 20(127):469–481.
31. Rondon L, Pouliquen O, Aussillous P (2011) Granular collapse in a fluid: role of the initial volume fraction. *Physics of Fluids* 23(7):073301.
32. Hellman N, Boesch T, Melvin E (1952) Starch granule swelling in water vapor sorption. *Journal of the American Chemical Society* 74(2):348–350.
33. Freundlich H, Röder H (1938) Dilatancy and its relation to thixotropy. *Transactions of the Faraday Society* 34:308–316.
34. Waduge RN, Xu S, Bertoff E, Seetharaman K (2013) Exploring the surface morphology of developing wheat starch granules by using atomic force microscopy. *Starch-Stärke* 65(5-6):398–409.
35. Vigil G, Xu Z, Steinberg S, Israelachvili J (1994) Interactions of silica surfaces. *Journal of Colloid and interface science* 165(2):367–385.
36. Israelachvili JN (2011) *Intermolecular and surface forces*. (Academic press).
37. Valmacco V et al. (2016) Dispersion forces acting between silica particles across water: influence of nanoscale roughness. *Nanoscale Horizons* 1(4):325–330.
38. Watanabe H et al. (1999) Nonlinear rheology of concentrated spherical silica suspensions: 3. concentration dependence. *Rheologica acta* 38(1):2–13.
39. Boersma WH, Laven J, Stein HN (1990) Shear thickening (dilatancy) in concentrated dispersions. *AIChE Journal* 36(3):321–332.
40. Lootens D, Van Damme H, Hémar Y, Hébraud P (2005) Dilatant flow of concentrated suspensions of rough particles. *Physical review letters* 95(26):268302.
41. Phung TN, Brady JF, Bossis G (1996) Stokesian dynamics simulation of brownian suspensions. *Journal of Fluid Mechanics* 313:181–207.
42. Brown E, Jaeger HM (2012) The role of dilation and confining stresses in shear thickening of dense suspensions. *Journal of Rheology* 56(4):875–923.
43. Fall A et al. (2015) Macroscopic discontinuous shear thickening versus local shear jamming in cornstarch. *Physical review letters* 114(9):098301.
44. Fall A, Lemaître A, Bertrand F, Bonn D, Ovarlez G (2010) Shear thickening and migration in granular suspensions. *Physical review letters* 105(26):268303.
45. Fernandez N et al. (2013) Microscopic mechanism for shear thickening of non-brownian suspensions. *Physical review letters* 111(10):108301.
46. Alexander AW et al. (2006) Avalanching flow of cohesive powders. *Powder Technology* 164(1):13–21.
47. Liu P, Yang R, Yu A (2011) Dynamics of wet particles in rotating drums: effect of liquid surface tension. *Physics of fluids* 23(1):013304.